Electroweak interactions in chiral molecules: Two-component density functional theory study of vibrational frequency shifts in polyhalomethanes

Robert Berger, Jason L. Stuber

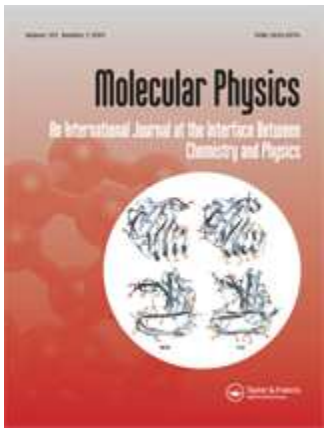

Electroweak interactions in chiral molecules: Two-component density functional theory study of vibrational frequency shifts in polyhalomethanes

Journal:	*Molecular Physics*
Manuscript ID:	TMPH-2006-0055
Manuscript Type:	Full Paper
Date Submitted by the Author:	09-Oct-2006
Complete List of Authors:	Berger, Robert; Johann Wolfgang Goethe-University, Frankfurt Institute for Advanced Studies (FIAS) Stuber, Jason; Johann Wolfgang Goethe-University, Frankfurt Institute for Advanced Studies (FIAS)
Keywords:	Molecular parity violation, Electroweak quantum chemistry, Polyhalomethanes, Vibrational frequency shifts, Zeroth order regular approximation

Molecular Physics, Vol. 00, No. 00, 0 Month 200x, 1–21

Electroweak interactions in chiral molecules: Two-component density functional theory study of vibrational frequency shifts in polyhalomethanes

Robert Berger*and Jason L. Stuber

Frankfurt Institute for Advanced Studies (FIAS), Johann Wolfgang Goethe-University,

Max-von-Laue-Straße 1, D-60438 Frankfurt am Main, Germany

(*Received 00 Month 200x; In final form 00 Month 200x*)

In this work a two-component density functional theory study of parity violation induced vibrational frequency shifts in chiral polyhalomethanes is reported and the prospects in these compounds to detect for the first time signals of parity violation in molecular systems are discussed. The recent synthesis and enantiomeric enrichment of CHClFI has renewed interest in examining electroweak corrections for this class of compounds. Utilising a (quasi-relativistic) two-component zeroth-order regular approximation approach to molecular parity violation together with density functional theory, parity violation induced relative vibrational frequency splittings $\Delta\nu_{\rm pv}/\nu$ between the C–F stretching fundamental of polyhalomethane enantiomers are computed. The relative splitting in CHClFI is raised compared to CHBrClF, for which upper bounds were determined experimentally. Given these bounds, however, the increase of the relative splitting is not sufficient. Instead the chiral methane derivative CHAtFI is considered which exhibits a significantly larger electroweak correction that induces vibrational frequency splittings on the order of the experimental resolution previously reported for CHBrClF. Employing compounds containing heavy nuclei such as astatine may, thus, be a necessity with present detection methods.

1 Introduction

Electroweak quantum chemistry presents a challenge and an opportunity for spectroscopy and theory [1]. Beyond relativistic corrections, effects of the fundamental weak force are also incorporated, which induce

*Corresponding author. Email: r.berger@fias.uni-frankfurt.de

Molecular Physics

ISSN 0026-8976 print/ ISSN 1362-3028 online

http://www.tandf.co.uk/journals

DOI: 10.1080/002689700xxxxxxxxxxx

tiny changes to molecular properties. This weak contribution is best elucidated in parity violation, the nonconservation of symmetry with respect to inversion of all particle coordinates, where non-identical mirror-image molecules (enantiomers) no longer have identical ground or excited state energies. While parity violating energy differences were predicted some forty years ago [2], providing a different perspective on the dynamics of chiral molecules (see *e.g.* Ref. [3]), their detection has still to be accomplished, despite previous experimental attempts (see *e.g.* Ref. [1, 4] and literature cited therein).

Perhaps the best studied candidate system for parity violation in polyatomic molecules is CHBrClF, the prototypical chiral methane derivative [5–9]. It has several advantages, namely it can be synthesised in sufficiently large quantities, its enantiomeric enrichment is possible and it possesses an intense infrared active C–F stretching mode amenable to CO_2 laser spectroscopy. The electroweak shift in rovibronic levels induces a splitting $\Delta\nu_{\mathrm{pv}}$ between transition frequencies of the left- and right-handed enantiomers, however the best experimental upper bound for relative rovibrational splittings $\Delta\nu_{\mathrm{pv}}/\nu$ reported for the C–F stretching fundamental of this compound (approximately 10^{-13}, see Ref. [7–9]) is about three orders of magnitude larger than theoretical estimates of the effect in CHBrClF [10–15].

While concerted efforts to detect molecular parity violation for the first time concern refinement of experiments, another front involves the choice of different candidate compounds. Chiral polyhalomethanes are a natural choice, related to CHBrClF by simple substitutions. While such derivatives can be probed theoretically [12, 14], synthesis of a specific chiral form is challenging. The recent synthesis and enantiomeric enrichment of CHClFI [16] has thus renewed interest in pursuing this candidate compound [17, 18], which is also one of our targets in the present study.

Previously, we have described our (quasi-relativistic) two-component zeroth-order regular approximation (ZORA) approach to molecular parity violation [19, 20], which we initially utilised to compute nuclear coordinate dependent parity violating (or parity odd) potentials in hydrogen peroxide and its heavier homologues, which contain sulfur, selenium, tellurium and polonium. We subsequently employed this approach to calculate parity violating energy differences in chiral pseudotetrahedral polyhalocubanes and corresponding vibrational frequency splittings in selected fundamentals of 1-bromo-3-chloro-5-fluorocubane [21].

In the present article we report our findings for the parity violating vibrational frequency splittings between the C–F stretching fundamentals of polyhalomethane enantiomers. Previous studies on molecular parity nonconservation involving chiral polyhalomethanes applied computational methods which accounted for electron correlation only in the investigation of CHBrClF [10, 11, 15]. These studies employed either multi-configurational linear response approaches to molecular parity violation starting from the (one-component) electronic Schrödinger equation (see Ref. [22]) or four-component approaches, involving second-order Møller-Plesset (MP2) perturbation theory (see Ref. [23]) and density functional theory (DFT) [15]. In this article we report the first parity odd potentials which include electron correlation effects for all chiral representatives of this class of compounds containing stable nuclei. Using the two-component DFT-ZORA approach [20], we also report the corresponding parity violation induced vibrational frequency splittings. As computed parity nonconservation effects in chiral molecules have currently the status of predictions, there is a high demand for going beyond the Hartree-Fock (HF) level of theory. Accurate and reliable theoretical predictions are of particular importance for the preparation and interpretation of future experiments that aim at the detection of molecular parity violation.

In addition to candidate polyhalomethanes which have been previously examined with electronic structure methods that neglect electron correlation [12, 14], we also consider the astatine containing derivative CHAtFI. Scaling laws [24–27] suggest that including proton-rich atomic centres, such as astatine, will enhance electroweak contributions. This is borne out in vertical substitution studies [12, 19, 20, 28–34], of which Ref. [32] also considered an astatine containing compound (NAtClF).

After providing an overview of the methodology in Section 2 and the specific computational details in Section 3, results of this study are presented in Section 4. Finally in Section 5 we give an outlook for measurement of molecular parity violation effects in the chiral methane derivatives.

2 Methodology

Our (quasi-relativistic) two-component ZORA approach to molecular parity violation has been described in detail in Refs. [19, 20]. Herein, we will only review its main features.

The starting point of the two-component DFT-ZORA approach [20] is the parity conserving four-component Dirac-Kohn-Sham (DKS) equation. In the form conventionally used in quantum chemistry [20, 35, 36], this is given by

$$\begin{pmatrix} V & c\vec{\sigma}\cdot\vec{p} \\ c\vec{\sigma}\cdot\vec{p} & V-2mc^2 \end{pmatrix} \begin{pmatrix} \phi_i \\ \chi_i \end{pmatrix} = \epsilon_i \begin{pmatrix} \phi_i \\ \chi_i \end{pmatrix} , \tag{1}$$

where

$$V = V_{\mathrm{nucl}} + J + V_{\mathrm{xc}} \, . \tag{2}$$

Here V_{nucl} is the electrostatic potential due to the nuclei, $J = J_{\phi\phi} + J_{\chi\chi}$ is the Coulomb operator and V_{xc} is the exchange correlation potential. The two-component spinors ϕ_i and χ_i represent respectively the upper and the lower components of the four-component DKS molecular orbital ψ_i corresponding to orbital energy ϵ_i. In Eq. (1), c denotes the speed of light, m the electron mass and $\vec{p}$ the linear momentum operator of the electron. The quantity $\vec{\sigma}$ is a vector consisting of the 2×2 Pauli spin matrices

$$\sigma_x = \begin{pmatrix} 0 & 1 \\ 1 & 0 \end{pmatrix} , \quad \sigma_y = \begin{pmatrix} 0 & -\mathrm{i} \\ \mathrm{i} & 0 \end{pmatrix} , \quad \sigma_z = \begin{pmatrix} 1 & 0 \\ 0 & -1 \end{pmatrix} , \tag{3}$$

with $\mathrm{i} = \sqrt{-1}$.

To arrive at the ZORA equations, the lower part of Eq. (1) is solved for χ_i using a regular series expansion for χ_i in terms of ϕ_i which is then truncated at zeroth-order. The potential terms appearing in the denominator are replaced by a model potential $\widetilde{V}$ [73]. Inserting the resulting approximate expression for χ_i

$$\chi_i \approx \frac{c}{2mc^2 - \widetilde{V}} \vec{\sigma}\cdot\vec{p}\,\phi_i \tag{4}$$

into the upper part of Eq. (1), one obtains the two-component DFT-ZORA equation

$$\left[V_\phi + \vec{\sigma}\cdot\vec{p} \frac{c^2}{2mc^2 - \widetilde{V}} \vec{\sigma}\cdot\vec{p} \right] \phi_i = \epsilon_i \phi_i \, , \tag{5}$$

where we have defined

$$V_\phi = V_{\rm nucl} + J_{\phi\phi} + V_{\rm xc}\,. \tag{6}$$

The Eq. (5) can be solved iteratively to obtain the orbital energies ϵ_i and two-component orbitals ϕ_i.

The exchange of virtual Z^0 bosons, which are one of the mediators of the weak force between elementary fermions, is (typically) the leading order contribution to parity violation in molecular systems with stable nuclei. In polyatomic molecules the largest contribution to parity violating energy differences stems from the weak interaction between electrons and nuclei, whereas interelectronic weak interactions are generally expected to be of minor importance. The effective four-component Hamiltonian $H_{\rm pv}^{\rm (e-nucl)}$ of the parity-violating electron-nucleus interactions (see for instance Refs. [1, 37, 38, 82]) is given by

$$\begin{aligned} H_{\rm pv}^{\rm (e-nucl)} &= H_{\rm pv}^{\rm (e-nucl,1)} + H_{\rm pv}^{\rm (e-nucl,2)} \\ &= \sum_{i=1}^{n} \left[h_{\rm pv}^{(1)}(i) + h_{\rm pv}^{(2)}(i) \right] \\ &= \frac{G_{\rm F}}{2\sqrt{2}} \sum_{i=1}^{n} \left[\sum_{A=1}^{N_{\rm nucl}} Q_{\rm w}(A) \gamma_i^5 \, \rho_A(\vec{r}_i) \right. \\ &\qquad \left. + \sum_{A=1}^{N_{\rm nucl}} \kappa_A \, \vec{\alpha}_i \cdot \vec{I}_A \, \rho_A(\vec{r}_i) \right], \end{aligned} \tag{7}$$

with n denoting the number of electrons and $N_{\rm nucl}$ the number of nuclei of the system. Here $G_{\rm F}$ represents Fermi's constant, $Q_{\rm w}(A) \approx (1 - 4\sin^2\theta_{\rm w})Z_A - N_A$ the weak charge of the nucleus A with nuclear charge number Z_A and number of neutrons N_A and $\sin^2\theta_{\rm w}$ the Weinberg parameter. $\vec{I}_A$ and $\rho_A(\vec{r}_i)$ respectively refer to the dimensionless nuclear spin operator and the normalised nucleon density distribution of nucleus A with $\vec{r}_i$ denoting the position vector of electron i. The 4×4 matrices $\vec{\alpha}_i$ and γ_i^5 act on electron i and are, in the representation employed herein, given by

$$\vec{\alpha} = \begin{pmatrix} \mathbf{0} & \vec{\sigma} \\ \vec{\sigma} & \mathbf{0} \end{pmatrix} \quad \text{and} \quad \gamma^5 = \begin{pmatrix} \mathbf{0} & \mathbf{1} \\ \mathbf{1} & \mathbf{0} \end{pmatrix}. \tag{8}$$

All prefactors entering the nuclear spin-dependent term in Eq. (7) (including contributions resulting from

the nuclear anapole moment [39]) are absorbed into the constant κ_A (see Refs. [38, 40] for some approximate formulae). The nuclear spin-dependent contribution $H_{\rm pv}^{({\rm e-nucl},2)}$ plays a key role for parity violating differences in Mössbauer, nuclear magnetic resonance (NMR) and electron paramagnetic resonance (EPR) spectra of chiral molecules [27, 41–51]. The dominant contribution to the parity-violating energy differences in ordinary chiral molecules, however, is expected to be caused by the nuclear spin-independent part $H_{\rm pv}^{({\rm e-nucl},1)}$. Therefore, $H_{\rm pv}^{({\rm e-nucl},2)}$ is neglected in the present work.

In the DKS treatment, the leading contribution to the parity violating potential in chiral molecules can be obtained to first order in $G_{\rm F}$ as the expectation value of $H_{\rm pv}^{({\rm e-nucl},1)}$

$$\begin{aligned} V_{\rm pv} &\approx \sum_i^{N_{\rm occ}} \left\langle \psi_i | h_{\rm pv}^{({\rm e-nucl},1)} | \psi_i \right\rangle \\ &= \sum_i^{N_{\rm occ}} \left\{ \langle \phi_i | f'_{\rm pv} | \chi_i \rangle + \langle \chi_i | f'_{\rm pv} | \phi_i \rangle \right\} , \end{aligned} \tag{9}$$

where

$$f'_{\rm pv} = \sum_{A=1}^{N_{\rm nucl}} G_{\rm F} Q_{\rm w}(A) \rho_A(\vec{r}) / (2\sqrt{2}) , \tag{10}$$

and the sum in Eq. (9) extends over the $N_{\rm occ}$ occupied Kohn-Sham orbitals.

If one uses the DFT ZORA approximation to relate the upper and the lower components, the parity violating potential to first order in $G_{\rm F}$ is given by

$$\begin{aligned} V_{\rm pv} \approx \sum_i^{\rm occ} & \left\langle \phi_i | f'_{\rm pv} \frac{c}{2mc^2 - \widetilde{V}} \vec{\sigma} \cdot \vec{p} | \phi_i \right\rangle \\ & + \left\langle \phi_i | \vec{\sigma} \cdot \vec{p} \frac{c}{2mc^2 - \widetilde{V}} f'_{\rm pv} | \phi_i \right\rangle , \end{aligned} \tag{11}$$

where $\{\phi_i\}$ are the self-consistent solutions of the ZORA equations (5). In the related Hartree-Fock version of the two-component ZORA approach, the exchange correlation potential in Eq. (5) is replaced by the Hartree-Fock exchange contribution for the upper component. Note that in our two-component HF-ZORA approach, the additional exchange terms $K_{\phi\chi}$ and $K_{\chi\phi}$ which couple upper and lower components are neglected (see Ref. [20] for a discussion).

We utilize Eq. (11) to compute the parity violating potential $V_{\rm pv}$ at a given (clamped) nuclear arrangement. The parity violating potential energy hypersurface is then given by $V_{\rm pv}$ as a function of the nuclear coordinates $\vec{q}$. In first order perturbation theory this additional potential gives rise to a parity violating shift of the nth vibrational energy level of a given enantiomer (R or S) according to (see also Ref. [11])

$$E_{n,\rm pv}^{(R,S)} \approx \langle \Psi_n^{(R,S)} | V_{\rm pv} | \Psi_n^{(R,S)} \rangle \, . \tag{12}$$

Here $|\Psi_n^{(R,S)}\rangle$ denotes the nth vibrational state of the R- and S-enantiomer, respectively, which are obtained by solving the parity conserving rovibrational Schrödinger equation for each enantiomer. For these states, $\mathcal{P}|\Psi_n^{(R)}\rangle = |\Psi_n^{(S)}\rangle$ holds, with $\mathcal{P}$ representing the parity operator. As $V_{\rm pv}$ is parity odd, the expectation values $E_{n,\rm pv}^{(R)}$ and $E_{n,\rm pv}^{(S)}$ have precisely the same magnitude but opposite sign. The corresponding energy difference between the nth vibrational levels of the two enantiomers is thus

$$E_{n,\rm pv}^{(S)} - E_{n,\rm pv}^{(R)} \approx 2 \langle \Psi_n^{(S)} | V_{\rm pv} | \Psi_n^{(S)} \rangle \, . \tag{13}$$

This approach assumes that the tunneling splitting between the hypothetical delocalised vibrational eigenstates (of opposite parity) of the parity conserving molecular Hamiltonian is much smaller than the parity violating coupling matrix element between these two states. This can, however, be assumed to be the case for the lowest vibrational levels in molecules which have a large barrier for stereomutation (see *e.g.* Ref. [3]).

In the separable anharmonic adiabatic approximation (SAAA), which was described in detail in Ref. [11] and applied for example in Refs. [52–55], the multidimensional integrals are simplified by approximating the zeroth-order vibrational wavefunctions by a direct product

$$|\Psi_n\rangle \approx |n_1, n_2, \ldots, n_{3N_{\rm nucl}-6}\rangle \, , \tag{14}$$

of one-dimensional anharmonic wavefunctions computed for one-dimensional cuts along the dimensionless reduced normal coordinates (q_j) through the multi-dimensional parity conserving potential energy hypersurface. The parity violating potential is also assumed to be separable in the normal coordinate

picture

$$V_{\mathrm{pv}}(\vec{q}) \approx \sum_{j}^{3N_{\mathrm{nucl}}-6} V_{\mathrm{pv}}(q_j)\,. \tag{15}$$

In this framework, the parity violating frequency shift ν_{pv} for a given vibrational transition of an enantiomer is obtained via

$$h\nu_{\mathrm{pv}}^{(R,S)} \approx \sum_{j=1}^{3N_{\mathrm{nucl}}-6} \Big[\langle {n'_j}^{(R,S)}|V_{\mathrm{pv}}(q_j)|{n'_j}^{(R,S)}\rangle - \langle {n_j}^{(R,S)}|V_{\mathrm{pv}}(q_j)|{n_j}^{(R,S)}\rangle\Big]\,, \tag{16}$$

with $\{n'_j\}_{j=1}^{3N_{\mathrm{nucl}}-6}$ and $\{n_j\}_{j=1}^{3N_{\mathrm{nucl}}-6}$ denoting the final and initial vibrational quantum numbers, respectively, of the one-dimensional anharmonic oscillator for the jth normal coordinate. The corresponding parity violating vibrational frequency splitting is then given by

$$\Delta\nu_{\mathrm{pv}} = \nu_{\mathrm{pv}}^{(S)} - \nu_{\mathrm{pv}}^{(R)} = 2\nu_{\mathrm{pv}}^{(S)}\,. \tag{17}$$

3 Computational Details

Geometry optimisations and harmonic force field calculations were performed with the Gaussian 03 software package [56] using the coupled cluster approach with single, double and non-iterative triple excitations, *i.e.* CCSD(T), including all electrons within the correlation treatment except those encompassed by the relativistic pseudopotentials. Period 1–3 atoms (H,C,F,Cl) employed the correlation-consistent polarised double zeta basis set (cc-pVDZ) [57, 58]. Period 4–6 atoms (Br, I and At) employed the large core scalar relativistic pseudopotentials (Br, I: [59], At: [60]) together with energy optimised valence basis sets with a (4s,4p)/[2s,3p] contraction on Br, I [61] and a (4s,4p,1d)/[2s,2p,1d] contraction on At [60] (see also [14]). In all cases tight geometry optimisation criteria were taken, ensuring gradient norms of less than $1.5 \times 10^{-5} E_{\mathrm{h}} a_0^{-1}$.

For all polyhalomethanes under consideration the parity violating potential V_{pv} of the S-enantiomer was evaluated using our two-component ZORA approach to molecular parity violation [19, 20] with Hartree-

Fock and density functional theory at the CCSD(T) optimised equilibrium geometry. At the DFT level the local density approximation (LDA) [62–64], gradient corrected B-LYP functional containing Becke's generalised gradient approximation functional for the exchange contribution [65] together with the Lee-Yang-Parr correlation contribution [66], and hybrid functional B3LYP [63, 65–69] were employed, the latter also using the local correlation approach as recommended in Ref. [63]. Our specific ZORA approach to molecular parity violation is incorporated within a modified TURBOMOLE [70, 71] version. Within the ZORA procedure the cc-pVDZ basis augmented with additional diffuse functions [72], *i.e.* aug-cc-pVDZ, was utilised in uncontracted form for hydrogen atoms while even-tempered basis sets, as described in [21], were employed for C, F, Cl, Br and I. For astatine we used the even-tempered basis set previously employed for polonium [19, 20, 33]. In this work we employ Fermi's constant value of $G_{\mathrm{F}} = (2.22254 \times 10^{-14}) E_{\mathrm{h}} a_0^3$ and a Weinberg parameter value of $\sin^2(\theta_{\mathrm{W}}) = 0.2319$ for comparison with previous studies.

To alleviate gauge-dependence of the ZORA method, van Wüllen's model potential approach [73] with additional damping [74] was used. This damping was also employed in our previous studies [19–21]. Parameters for the model densities are reported in Ref. [21] and we provide the data for astatine in the supplementary material. A dense integration grid with a total number of 10000 radial shells was employed in all ZORA calculations for numerical quadrature of one-electron integrals involving the model potential. A Gaussian nuclear model with the standard exponents, as given in Ref. [75], was employed in ZORA calculations for the isotopes ^{1}H, ^{12}C, ^{19}F, ^{35}Cl, ^{79}Br, ^{127}I and ^{210}At. Convergence criterion for the energy was $|\Delta E| < 10^{-6}\, E_{\mathrm{h}}$ between subsequent iterations, however this was not sufficient to ensure convergence of the parity violation potential, and an auxiliary condition requiring a relative change of the spin-orbit coupling contribution to the total energy at a level of 10^{-12} was enforced.

In those molecules where the parity violating induced relative splitting for the C–F stretching fundamental was also calculated within the separable anharmonic adiabatic approximation (SAAA) [11], geometries corresponding to excursions along the dimensionless reduced normal coordinates q_j corresponding to the C–F stretching mode were generated with Cartesian force field data from Gaussian 03 force field calculations employing numerical differentiation of the energy, having step size 0.01Å. Normal coordinates were

obtained with the hotFCHT [76] software.

Geometries corresponding to excursions along the C–F stretching normal coordinate were employed to generate a one-dimensional cut through the nine-dimensional (parity conserving) CCSD(T) potential energy surface. The value $q_j = 0$ corresponds to the optimised equilibrium geometry, and each one-dimensional cut was evaluated at 75 points from $q_j = -5 \ldots 5$, with spacings of 0.05 closest to equilibrium and 0.5 at the endpoints. Data for the potential energy curve was then splined with cubic polynomials, using the Mathematica 5.2 software package [77], to a regular grid with spacing of 0.05 units. The resulting surface was then exploited to calculate, using a discrete variable representation [78], vibrational energies, wavefunctions and the expectation values $\langle n_j|q_j^k|n_j\rangle$ with $k = 1, \ldots, 4$ for each vibrational level $|n_j\rangle$ with quantum number n_j.

In those chiral methane derivatives, one-dimensional cuts $V_{\mathrm{pv}}(q)$ through the nine-dimensional parity violating potential energy surface along the C–F stretching normal coordinate were also evaluated at 17 points from $q_j = -3 \ldots 3$, with finest spacing near the equilibrium geometry. The resulting data points for the potential were fit with an, at most, fourth-order polynomial using Mathematica. These coefficients together with the previously calculated vibrational expectation values $\langle n_j|q_j^k|n_j\rangle$ were then employed to determine the vibrational splitting $\Delta\nu_{\mathrm{pv}}$ corresponding to the frequency difference between the C–F stretching fundamental of the enantiomers. Relative splittings $\Delta\nu_{\mathrm{pv}}/\nu$ were then formed by dividing with the frequency ν of this fundamental.

4 Results and Discussion

The calculated value of the parity violating potential V_{pv} at the equilibrium geometry for each polyhalomethane and each computational method under consideration is provided in Tab. 1. For a subset of these chiral methane derivatives we also computed the relative parity violating vibrational frequency splitting $\Delta\nu_{\mathrm{pv}}/\nu$ for the C–F stretching fundamental, as given in Tab. 2. Additional raw and fitted data is located in the supplementary material.

At the CCSD(T) optimised equilibrium geometry the parity violating potential V_{pv} (*cf.* Tab. 1) depends

Table 1. Parity violating potential $V_{\rm pv}/hc$ at the CCSD(T) optimised geometry of the S–enantiomer. Entries are in units of $10^{-12}\,{\rm cm}^{-1}$.

	Molecule	HF	B3LYP	B–LYP	LDA
1	CHBrClF	−1.45	−0.39	+0.18	+0.53
2	CHBrClI	−24.7	−7.84	+3.93	+8.96
3	CHBrFI	−38.5	−7.94	+10.3	+19.4
4	CHClFI	−13.7	−3.34	+2.63	+5.36
5	CBrClFI	+5.12	+1.21	−0.89	−2.21
6	CHAtFI	−2315.	−299.	+666.	+966.

strongly on the choice of density functional, affecting not just the magnitude of $V_{\rm pv}$ but also the sign. These findings are in contrast to our previous density functional calculations [20] of parity violating potentials in the series of molecules H_2X_2; $X = O, S, Se, Te, Po$, where different functionals gave consistent electron correlation corrections to the parity violating potential. The present results clearly indicate that functional variability is a more general trend in polyhalomethanes and not restricted only to CHBrClF, for which it was reported recently in a four-component study [15] (see also figure 3 in Ref. [79] where preliminary results obtained in a non-relativistic uncoupled DFT framework are displayed). Despite the functional dependence of $V_{\rm pv}$, an overall ordering going from HF, B3LYP, B-LYP to LDA is exhibited in all systems examined. In this work the order persists at both equilibrium and C–F stretched geometries (see *e.g.* Fig. 1).

We note in passing that in electronic g-tensors, which like parity violating potentials crucially depend on the spin-orbit coupling, a pronounced dependence on the choice of functional and in particular amount of Hartree-Fock exchange contribution of hybrid DFT schemes has been observed for transition metal complexes (see for instance Ref. [80]). For main group compounds however, typically only limited and systematic shifts have been reported, in contrast to what we presently observe for polyhalomethane parity

violating potentials.

The parity violating potential V_{pv} at the equilibrium geometry determines to first approximation the energy difference ΔE_{pv} between the enantiomers ($|\Delta E_{\mathrm{pv}}| \approx 2|V_{\mathrm{pv}}|$). For each method we observe a relative ordering of the potential $|V_{\mathrm{pv}}|$ from $\mathbf{3} > \mathbf{2} > \mathbf{4} > \mathbf{5} > \mathbf{1}$. This polyhalomethane sequence corresponds directly with their polyhalocubane counterparts, as noted by Fokin *et al.* [21], albeit with significantly larger magnitude than in the polyhalocubanes, which is important information for rational design of compounds with large $|V_{\mathrm{pv}}|$. Utilising $|V_{\mathrm{pv}}|$ in CHBrClF (**1**) as a reference point, we would then predict an order of magnitude increase in the electroweak splitting for the recently synthesised CHClFI (**4**) and a significant three orders of magnitude increase in CHAtFI (**6**).

Parity violating potentials obtained previously by Schwerdtfeger *et al.* [14] in a four-component Dirac-Hartree-Fock-Coulomb (DHFC) framework are systematically smaller in magnitude than the present HF values of V_{pv} in **1**–**5** and the density functional data for V_{pv} in compound **1**. This can be ascribed to the smaller basis sets used in the previous study. We expect the slightly different equilibrium geometries and the use of the model potential $\tilde{V}$ to cause only minor deviations ($\lesssim 5\%$).

In both the previous DHFC and the present two-component HF framework, contributions from the Breit interaction have been neglected. While the importance of this interaction term in the accurate description of parity violating potentials will be discussed in detail elsewhere [81], we expect the neglect of the Breit contribution to cause relative errors of less than 10% in the systems studied here, with deviations expected to be largest in magnitude for CHBrClF. We note in passing that relative deviations of more than 10% can, however, not be excluded at geometries where the parity violating potentials almost vanish. Further corrections from quantum electrodynamics and from nuclear size effects, as well as contributions from the neglected nuclear spin-dependent term and the two-electron term of the parity violating Hamiltonian are (typically) expected to be much smaller, perhaps on the sub-percent level. Such estimates are based on the experience in atomic parity violation calculations (see for instance Refs. [37, 82]). One of our future research projects involves the explicit calculation of these effects.

Vibrational spectroscopy is one means to probe parity violating effects in chiral molecules, and in Tab. 2

Table 2. Parity violating relative vibrational frequency splittings $\Delta\nu_{\rm pv}/\nu$ between the C–F stretching fundamental of the S– and R–enantiomers ($\Delta\nu_{\rm pv} = \nu^S_{\rm pv} - \nu^R_{\rm pv}$). Values are dimensionless and are given in multiples of 10^{-16}.

	Molecule	HF	B3LYP	B–LYP	LDA
1	CHBrClF	+0.72	+1.01	+0.93	+0.98
3	CHBrFI	+17.8	+22.9	+22.1	+24.1
4	CHClFI	+9.35	+8.96	+6.94	+7.39
6	CHAtFI	−1073.	−1009.	−851.	−946.

we provide the calculated relative parity violating vibrational frequency splittings $\Delta\nu_{\rm pv}/\nu$ between the C–F stretching fundamental of the enantiomers for a subset of the chiral methane derivatives (**1**,**3**,**4**,**6**). The computed C–F stretching fundamental has $\tilde{\nu} = 1079\,{\rm cm}^{-1}$ to $1104\,{\rm cm}^{-1}$ in these compounds and is in the ideal range for CO_2 laser vibrational spectroscopy.

Given the significant differences between parity violating potentials at the equilibrium geometry, depending on choice of functional, one might expect the corresponding relative shifts are similarly affected, a feature which is not borne out by the data. Indeed, the spread between vibrational frequency relative shifts is about twenty percent from the average for a given choice of molecule. In the lighter polyhalomethanes studied herein (**1**, **3**, **4**) it can in part be ascribed to the predominantly linear dependence of the parity violating potential along the C–F stretching normal mode and an almost functional-independent value for the slope (see Fig. 1), parallelling the slight variation in slope found previously in the Breit-Pauli framework within the random phase approximation (RPA) and the complete active space-self consistent field (CASSCF) method [11]. While in molecules **4** and **6** the spread of $\Delta\nu_{\rm pv}/\nu$ predicted with the various functionals is larger than the correlation correction predicted at the B3LYP level, all functionals reduce the magnitude of the splitting. In case of molecules **1** and **3**, DFT provides a consistent picture, with correlation corrections on the order of about thirty percent.

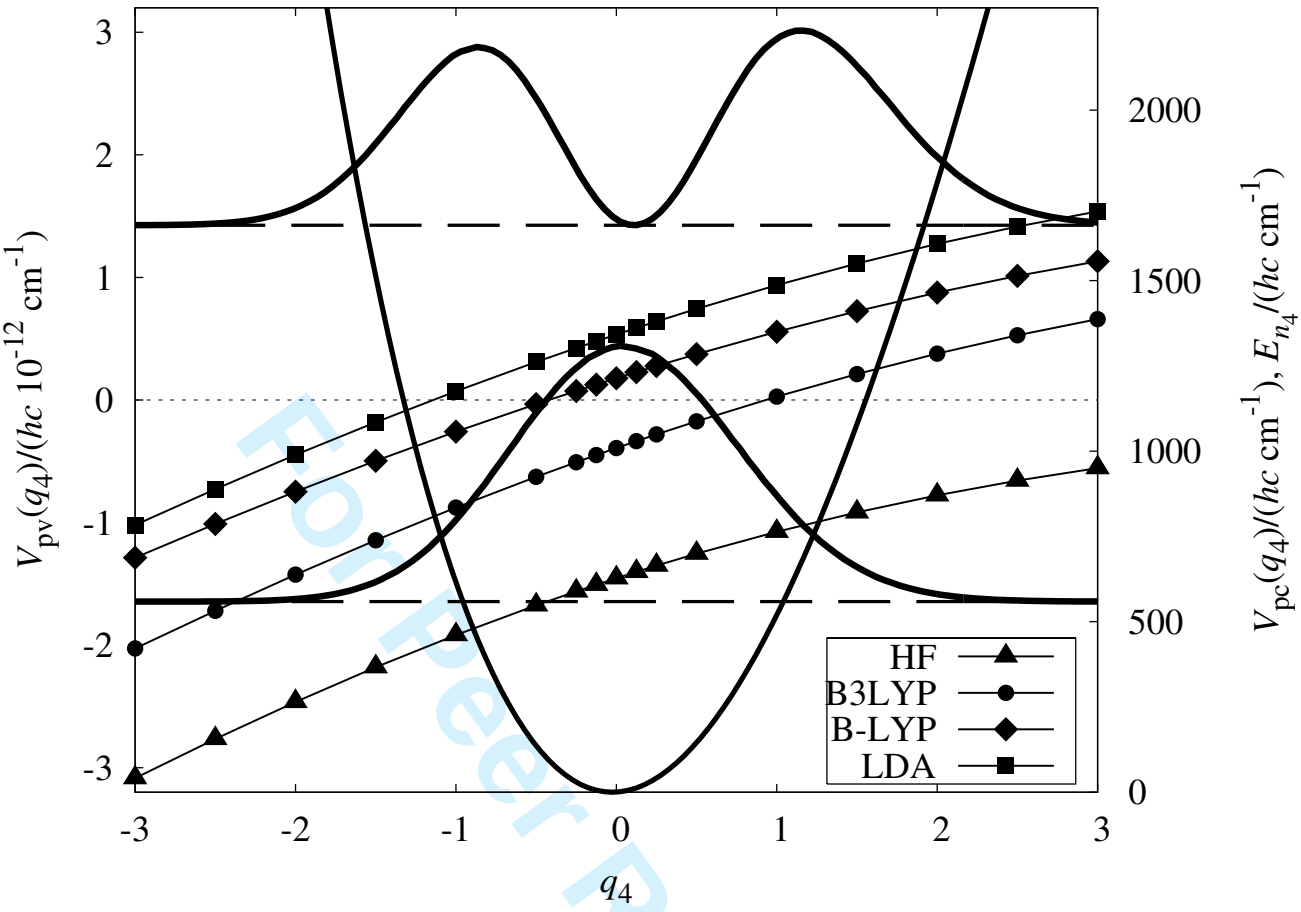

Figure 1. Parity violating potentials $V_{\rm pv}(q_4)$ (solid lines with triangles, bullets, diamonds or squares; left ordinate), parity conserving potential $V_{\rm pc}(q_4)$ (solid curve; right ordinate) and parity conserving anharmonic vibrational energy eigenvalues E_n (dashed, thick horizontal lines, right ordinate) of (*S*)-CHBrClF as a function of the dimensionless reduced normal coordinate q_4 corresponding to the C–F stretching normal mode. Additionally, the probability density $|\langle q_4|n_4\rangle|^2$ of the one-dimensional vibrational states with quantum numbers $n_4 = 0, 1$ is shown, in arbitrary units.

As a measure of the significance required in practice for candidate compounds, the most recently reported experimental upper bound in the study of CHBrClF (see Ref. [7–9]) was $\Delta\nu_{\rm pv}/\nu \lesssim 10^{-13}$. In CHBrClF (**1**) the predicted relative splitting is on the order of $\Delta\nu_{\rm pv}/\nu \approx 10^{-16}$, still three orders of magnitude smaller than reported experimental viability. Any compound which can significantly enhance the parity violating frequency shifts should be taken under serious consideration. Substitution with iodine increases the parity violation induced effect in both CHClFI (**4**) and CHBrFI (**3**), and hence both are desirable, however even in these candidates $\Delta\nu_{\rm pv}/\nu$ is still two orders of magnitude too small under the conditions reported in Refs. [7–9].

In the astatine derivative CHAtFI (**6**) the relative splitting is as large as $\Delta\nu_{\rm pv}/\nu \approx 10^{-13}$ and therefore

already comparable to reported experimental resolution. Most notably, this splitting is an order of magnitude larger than the splittings computed recently for the chiral methane derivatives ClHgCHFCl and $PH_3AuCHFCl$ by Bast and Schwerdtfeger [83], who had concluded that it would be difficult to achieve much higher values for parity violating effects in C–F stretching modes. Our results, in contrast, imply that there is still room for significant further increase, which is extremely encouraging for future experiments. The use of astatine compounds would impose however severe experimental constraints, due to abundance and lifetime. Of the various astatine isotopes, the most stable known isotopes have half-lives on the order of a few hours with availabilities at the microgram level [84, 85]. Nevertheless this theoretical compound CHAtFI still provides a reference value of the magnitude for chiral methane derivatives containing period six nuclei. The effect is significant, and indicates that the potential of period six or even seven substituents has yet to be fully explored.

5 Conclusions and Outlook

In this work we calculated the parity violating potential for CHBrClF and first results including electron correlation effects in other polyhalomethanes within the framework of quasi-relativistic density functional theory. Parity violating contributions were computed utilising the two-component ZORA approach, employing extended even-tempered basis sets together with the HF and DFT (LDA, B-LYP and B3LYP) methodologies. Determination of the corresponding vibrational frequency shifts was performed in the SAAA [11].

Inclusion of electron correlation is essential for accurate and reliable prediction of electroweak effects. We have illustrated through our evaluation of the parity violating potential at the equilibrium geometry that a relative ordering between functionals is observed in the polyhalomethanes, however, the choice of functional changes both the value of the parity violating potential and also the sign. An account of correlation effects beyond density functional theory, at least with the given choice of functionals, thus seems unavoidable when establishing size and sign of the parity violating energy difference between polyhalomethane enantiomers. In the case of CHBrClF, previous CASSCF [11] and MP2 [15] calculations favour the *S*-enantiomer, yielding

correlation corrections which are smaller in magnitude than those computed at the B3LYP level, but of identical sign (except for one choice of active space). Further investigations utilising higher level electron correlation treatments are therefore required to provide a conclusive answer on the parity violating energy difference between the R– and S–forms.

By virtue of the significant differences between parity violating potentials at the equilibrium structures, one might have expected that corresponding vibrational frequency shifts are similarly affected. Since the relative ordering is preserved also at the extended geometries studied herein, however, one observes instead correlation corrections of consistent sign for the parity violating frequency splittings between the C-F stretching fundamentals of the polyhalomethane enantiomers studied herein. While in CHClFI and CHAtFI the spread of $\Delta\nu_{\rm pv}/\nu$ predicted with the various functionals (on a 20% level) is larger than the correlation correction predicted at the B3LYP level, DFT provides for CHBrClF and CHBrFI a consistent picture with correlation corrections on the order of about thirty percent. Previous correlation corrections found on the CASSCF level [11] and on the four-component MP2 and DFT level [15] for CHBrClF agree well with this finding.

Beyond the treatment of electronic structure, a more accurate theoretical study would also require improvement of the vibrational structure, including anharmonic couplings for either a subset [86] or all vibrational modes. While this is outside the scope of the present investigation, our ZORA approach to molecular parity violation can also be utilised to compute the fully coupled 9-dimensional parity violating potential energy hypersurface. If supported at select structures by a few high-level benchmark calculations with systematically improvable electron-correlating methods, such as multi-configurational approaches or coupled cluster methods, the accurate prediction of parity violating vibrational shifts required for the interpretation of future experiments is possible.

The relative parity violating vibrational frequency splitting $\Delta\nu_{\rm pv}/\nu$ between the C–F stretching fundamental for the enantiomers of CHBrClF obtained in this study is on the order of 10^{-16}, largely independent of the choice of functional employed, and is still approximately three orders of magnitude smaller than the experimental upper bound of $\Delta\nu_{\rm pv}/\nu \lesssim 10^{-13}$. Substitution with iodine enhances $\Delta\nu_{\rm pv}/\nu$, however

an increase of resolving power by at least two orders of magnitude compared to Refs. [7, 9] would still be required to experimentally detect such a parity violation induced splitting in chiral molecules.

To achieve larger relative splittings, we also consider candidate molecules which contain atomic constituents with larger nuclear charges, in accordance with the scaling law behaviour. We examined the CHAtFI molecule, which has a parity violation induced relative vibrational splitting approximately one thousand times larger than that of CHBrClF, placing it in the range of present experimental resolution. While this system has many desirable features, difficulties such as availability, synthesis, enantiomeric enrichment and in particular lifetime are significant obstacles. Nevertheless it signals that experimental viability, under present conditions for the polyhalomethanes, seems to require the use of period six elemental substituents, which might also translate to other spectroscopic techniques. The CHAtFI molecule provides a hint of the parity violating relative splitting effect size for the C–F stretching fundamental in similar systems.

Acknowledgements

Discussions with Jürgen Stohner and Sophie Nahrwold are gratefully acknowledged. This work was supported by the Volkswagen Foundation. We also acknowledge the HLRN and the CSC Frankfurt for access to their computing facilities.

References

[1] R. Berger, in *Relativistic Electronic Structure Theory, Part: 2, Applications*, edited by P. Schwerdtfeger (Elsevier, Netherlands, 2004), pp. 188–288.

[2] Y. Yamagata, J. Theor. Biol. **11**, 495 (1966).

[3] R. Berger, M. Gottselig, M. Quack, and M. Willeke, Angew. Chem. Int. Ed. **40**, 4195 (2001).

[4] M. Quack, Angew. Chem. Int. Ed. **41**, 4618 (2002).

[5] O. N. Kompanets, A. R. Kukudzhanov, V. S. Letokhov, and L. L. Gervits, Opt. Commun. **19**, 414 (1976).

[6] A. Bauder, A. Beil, D. Luckhaus, F. Müller, and M. Quack, J. Chem. Phys. **106**, 7558 (1997).

[7] C. Daussy, T. Marrel, A. Amy-Klein, C. T. Nguyen, C. J. Bordé, and C. Chardonnet, Phys. Rev. Lett. **83**, 1554 (1999).

[8] T. Marrel, M. Ziskind, C. Daussy, and C. Chardonnet, J. Mol. Struct. **599**, 195 (2001).

[9] M. Ziskind, C. Daussy, T. Marrel, and C. Chardonnet, Eur. Phys. J. D **20**, 219 (2002).

[10] M. Quack and J. Stohner, Phys. Rev. Lett. **84**, 3807 (2000).

[11] M. Quack and J. Stohner, Z. Phys. Chem. **214**, 675 (2000).

[12] J. K. Laerdahl, P. Schwerdtfeger, and H. M. Quiney, Phys. Rev. Lett **84**, 3811 (2000).

[13] R. G. Viglione, R. Zanasi, P. Lazzeretti, and A. Ligabue, Phys. Rev. A **62**, 052516 (2000).

[14] P. Schwerdtfeger, J. K. Laerdahl, and C. Chardonnet, Phys. Rev. A **65**, 042508 (2002).

[15] P. Schwerdtfeger, T. Saue, J. N. P. van Stralen, and L. Visscher, Phys. Rev. A **71**, 012103 (2005).

[16] J. Crassous, Z. J. Jiang, and P. L. Polavarapu, Tetrahedron: Asymmetry **15**, 1995 (2004).

[17] J. Cuisset, J. R. A. Moreno, T. R. Huet, D. Petitprez, J. Demaison, and J. Crassous, J. Phys. Chem. A **109**, 5708 (2005).

[18] P. Soulard, P. Asselin, A. Cuisset, J. R. A. Moreno, T. R. Huet, D. Petitprez, J. Demaison, T. B. Freedman, X. L. Cao, L. A. Nafie, et al., Phys. Chem. Chem. Phys. **8**, 79 (2006).

[19] R. Berger, N. Langermann, and C. van Wüllen, Phys. Rev. A **71**, 042105 (2005).

[20] R. Berger and C. van Wüllen, J. Chem. Phys. **122**, 134316 (2005).

[21] A. A. Fokin, P. R. Schreiner, R. Berger, G. H. Robinson, P. Wei, and C. F. Campana, J. Am. Chem. Soc. **128**, 5332 (2006).

[22] R. Berger and M. Quack, J. Chem. Phys. **112**, 3148 (2000).

[23] J. N. P. van Stralen, L. Visscher, C. V. Larsen, and H. J. A. Jensen, Chem. Phys. **331**, 81 (2005).

[24] B. Y. Zel'dovich, D. B. Saakyan, and I. I. Sobel'man, JETP Lett. **25**, 94 (1977).

[25] R. A. Harris and L. Stodolski, Phys. Lett. B **78**, 313 (1978).

[26] D. W. Rein, R. A. Hegstrom, and P. G. H. Sandars, Phys. Lett. **71A**, 499 (1979).

[27] V. G. Gorshkov, M. G. Kozlov, and L. N. Labzowsky, Sov. Phys. JETP **55**, 1042 (1982).

[28] S. F. Mason and G. E. Tranter, Mol. Phys. **53**, 1091 (1984).

[29] L. Wiesenfeld, Mol. Phys. **64**, 739 (1988).

[30] P. Lazzeretti and R. Zanasi, Chem. Phys. Lett. **279**, 349 (1997).

[31] A. Bakasov, T.-K. Ha, and M. Quack, J. Chem. Phys. **109**, 7263 (1998).

[32] L. N. Ivanov and V. S. Letokhov, Dokl. Phys. **43**, 523 (1998).

[33] J. K. Laerdahl and P. Schwerdtfeger, Phys. Rev. A **60**, 4439 (1999).

[34] A. Bakasov, R. Berger, T.-K. Ha, and M. Quack, Int. J. Quantum Chem. **99**, 393 (2004).

[35] A. Rosen and D. E. Ellis, J. Chem. Phys. **62**, 3039 (1975).

[36] W. Klopper, J. H. van Lenthe, and A. C. Hennum, J. Chem. Phys. **113**, 9957 (2000).

[37] J. Sapirstein, in *Relativistic Electronic Structure Theory, Part: 1, Fundamentals*, edited by P. Schwerdtfeger (Elsevier, Netherlands, 2002), pp. 471–525.

[38] I. B. Khriplovich, *Parity Nonconservation in Atomic Phenomena* (Gordon and Breach Science Publ., Philadelphia, 1991).

[39] I. B. Zel'dovich, Sov. Phys. JETP **6**, 1184 (1958).

[40] V. V. Flambaum and I. B. Khriplovich, Sov. Phys. JETP **52**, 835 (1980).

[41] I. B. Khriplovich, Sov. Phys. JETP **52**, 177 (1980).

[42] I. B. Khriplovich, Z. Phys. A **322**, 507 (1985).

[43] A. L. Barra, J. B. Robert, and L. Wiesenfeld, Phys. Lett. A **115**, 443 (1986).

[44] A. L. Barra, J. B. Robert, and L. Wiesenfeld, Europhys. Lett. **5**, 217 (1988).

[45] A. L. Barra and J. B. Robert, Mol. Phys. **88**, 875 (1996).

[46] J. B. Robert and A. L. Barra, Chirality **13**, 699 (2001).

[47] G. Laubender and R. Berger, ChemPhysChem **4**, 395 (2003).

[48] A. Soncini, F. Faglioni, and P. Lazzeretti, Phys. Rev. A **68**, 033402 (2003).

[49] V. Weijo, P. Manninen, and J. Vaara, J. Chem. Phys. **123**, 054501 (2005).

[50] G. Laubender and R. Berger, Phys. Rev. A **74**, 032105 (2006).

[51] R. Bast, P. Schwerdtfeger, and T. Saue, J. Chem. Phys. **125**, 064504 (2006).

[52] R. Berger, M. Quack, and J. Stohner, Angew. Chem. Int. Ed. **40**, 1667 (2001).

[53] M. Quack and J. Stohner, Chirality **13**, 745 (2001).

[54] J. Stohner, Int. J. Mass. Spectr. **233**, 385 (2004).

[55] R. Berger, G. Laubender, M. Quack, A. Sieben, J. Stohner, and M. Willeke, Angew. Chem. Int. Ed. **44**, 3623 (2005).

[56] M. J. Frisch, G. W. Trucks, H. B. Schlegel, G. E. Scuseria, M. A. Robb, J. R. Cheeseman, J. A. Montgomery, Jr., T. Vreven, K. N. Kudin, J. C. Burant, et al., *Gaussian 03, Revision C.02*, Gaussian, Inc. , Wallingford, CT, 2004.

[57] T. H. Dunning, Jr., J. Chem. Phys. **90**, 1007 (1989).

[58] D. E. Woon and T. H. Dunning, Jr., J. Chem. Phys. **98**, 1358 (1993).

[59] P. Schwerdtfeger, M. Dolg, W. H. E. Schwarz, G. A. Bowmaker, and P. D. W. Boyd, J. Chem. Phys. **91**, 1762 (1989).

[60] W. Küchle, M. Dolg, H. Stoll, and H. Preuss, Mol. Phys. **74**, 1245 (1991).

[61] A. Bergner, M. Dolg, W. Küchle, H. Stoll, and H. Preuß, Mol. Phys. **80**, 1431 (1993).

[62] W. Kohn and L. J. Sham, Phys. Rev. **140**, 1133 (1965).

[63] S. H. Vosko, L. Wilk, and M. Nuisar, Can. J. Phys. **58**, 1200 (1980).

[64] P. A. M. Dirac, Proc. Cambridge Phil. Soc. **26**, 376 (1930).

[65] A. D. Becke, Phys. Rev. A **38**, 3098 (1988).

[66] C. Lee, W. Yang, and R. G. Parr, Phys. Rev. B **37**, 785 (1988).

[67] P. J. Stephens, F. J. Devlin, C. F. Chabalowski, and M. J. Frisch, J. Phys. Chem. **98**, 11623 (1994).

[68] A. D. Becke, J. Chem. Phys. **98**, 1372 (1993).

[69] A. D. Becke, J. Chem. Phys. **98**, 5648 (1993).

[70] R. Ahlrichs, M. Bär, M. Häser, H. Horn, and C. Kölmel, Chem. Phys. Lett. **162**, 165 (1989).

[71] M. Häser and R. Ahlrichs, J. Comput. Chem. **10**, 104 (1989).

[72] R. A. Kendall, T. H. Dunning, Jr., and R. J. Harrison, J. Chem. Phys. **96**, 6796 (1992).

[73] C. van Wüllen, J. Chem. Phys. **109**, 392 (1998).

[74] W. Liu, C. van Wüllen, F. Wang, and L. Li, J. Chem. Phys. **116**, 3626 (2002).

[75] L. Visscher and K. G. Dyall, At. Data Nucl. Data Tables **67**, 207 (1997).

[76] R. Berger, C. Fischer, and M. Klessinger, J. Phys. Chem. A **102**, 7157 (1998).

[77] Wolfram Research, Inc., *Mathematica* (2005), Wolfram Research, Inc. , Champaign, IL.

[78] R. Meyer, J. Chem. Phys. **52**, 2053 (1970).

[79] M. Quack and J. Stohner, Chimia **59**, 530 (2005).

[80] M. Kaupp, R. Reviakine, O. L. Malkina, A. Arbuznikov, B. Schimmelpfennig, and V. G. Malkin, J. Comput. Chem. **23**, 794 (2002).

[81] R. Berger and J. L. Stuber, (submitted for publication).

[82] S. A. Blundell, J. Sapirstein, and W. R. Johnson, Phys. Rev. D **45**, 1602 (1992).

[83] R. Bast and P. Schwerdtfeger, Phys. Rev. Lett. **91**, 023001 (2003).

[84] S. Lindebren, T. Bäck, and H. J. Jensen, Appl. Radiat. Isot. **55**, 157 (2001).

[85] O. Lebeda, R. Jiran, J. Ráliš, and J. Štursa, Appl. Radiat. Isot. **63**, 49 (2005).

[86] M. Quack and J. Stohner, J. Chem. Phys. **119**, 11228 (2003).

Supplementary Material

Electroweak interactions in chiral molecules: Two-component density functional theory study of vibrational frequency shifts in polyhalomethanes

R. Berger and J. L. Stuber

Frankfurt Institute for Advanced Studies (FIAS),
Johann Wolfgang Goethe-Universität,
D-60438 Frankfurt am Main, Germany

September 2006

1. CHBrClF

Table 1.1: Equilibrium geometry obtained at the CCSD(T) level for the S–enantiomer of CHBrClF. Coordinates are in ångström (Å).

Atom	x	y	z
C	+0.520423	+0.549491	+0.503314
H	+0.520423	+0.549491	+1.602514
F	+1.792767	+0.549491	+0.042270
Cl	−0.317441	+2.007488	−0.064263
Br	−0.376703	−1.112373	−0.078698

Table 1.2: Unscaled harmonic wavenumbers $\tilde{\omega}$ (in cm^{-1}) calculated at the CCSD(T) level of theory for the S–enantiomer of CHBrClF. The C–F stretch mode corresponds to mode ν_4.

Mode	$\tilde{\omega}$
ν_1	3170.5
ν_2	1334.4
ν_3	1236.4
ν_4	1122.1
ν_5	786.6
ν_6	638.4
ν_7	422.6
ν_8	309.2
ν_9	224.2

Table 1.3: Cartesian displacements (in Å) corresponding to a unit shift along the dimensionless reduced normal coordinate q_4 for the S–enantiomer of CHBrClF.

Atom	x	y	z
C	-6.3056×10^{-1}	$+6.8027 \times 10^{-3}$	$+2.6809 \times 10^{-1}$
H	-4.7696×10^{-1}	$+1.6461 \times 10^{-1}$	$+2.8155 \times 10^{-1}$
F	$+4.0506 \times 10^{-1}$	$+2.9482 \times 10^{-3}$	-1.8006×10^{-1}
Cl	$+8.4131 \times 10^{-3}$	-5.1426×10^{-3}	$+1.8118 \times 10^{-3}$
Br	$+7.3210 \times 10^{-4}$	-1.5676×10^{-3}	-1.8164×10^{-3}

Table 1.4: One dimensional cut through the CCSD(T) parity conserving potential energy hypersurface (V_{pc} in 10^3 Hartree (E_h)) along the dimensionless reduced normal coordinate (q_4) corresponding to the C–F stretching mode of the S–enantiomer of CHBrClF.

q	V_{pc}	q	V_{pc}
−5.00	−0.610907850	+0.05	−0.611042436
−4.50	−0.610942038	+0.10	−0.611042417
−4.00	−0.610969235	+0.15	−0.611042386
−3.50	−0.610990623	+0.20	−0.611042343
−3.00	−0.611007182	+0.25	−0.611042288
−2.80	−0.611012640	+0.30	−0.611042221
−2.60	−0.611017503	+0.35	−0.611042144
−2.40	−0.611021814	+0.40	−0.611042055
−2.20	−0.611025612	+0.45	−0.611041955
−2.00	−0.611028933	+0.50	−0.611041845
−1.80	−0.611031812	+0.55	−0.611041724
−1.60	−0.611034281	+0.60	−0.611041593
−1.50	−0.611035370	+0.65	−0.611041452
−1.40	−0.611036369	+0.70	−0.611041301
−1.30	−0.611037279	+0.75	−0.611041141
−1.20	−0.611038104	+0.80	−0.611040971
−1.10	−0.611038848	+0.85	−0.611040792
−1.00	−0.611039513	+0.90	−0.611040604
−0.95	−0.611039817	+0.95	−0.611040407
−0.90	−0.611040103	+1.00	−0.611040202
−0.85	−0.611040370	+1.10	−0.611039766
−0.80	−0.611040619	+1.20	−0.611039298
−0.75	−0.611040851	+1.30	−0.611038799
−0.70	−0.611041066	+1.40	−0.611038270
−0.65	−0.611041263	+1.50	−0.611037713
−0.60	−0.611041445	+1.60	−0.611037129
−0.55	−0.611041610	+1.80	−0.611035885
−0.50	−0.611041759	+2.00	−0.611034545
−0.45	−0.611041893	+2.20	−0.611033120
−0.40	−0.611042011	+2.40	−0.611031616
−0.35	−0.611042114	+2.60	−0.611030041
−0.30	−0.611042203	+2.80	−0.611028402
−0.25	−0.611042277	+3.00	−0.611026704
−0.20	−0.611042337	+3.50	−0.611022245
−0.15	−0.611042384	+4.00	−0.611017538
−0.10	−0.611042416	+4.50	−0.611012652
−0.05	−0.611042436	+5.00	−0.611007641
+0.00	−0.611042442		

Table 1.5: One dimensional cut through the ZORA parity violating potential energy hypersurface (V_{pv} in 10^{-17} Hartree (E_h)) along the dimensionless reduced normal coordinate (q_4) corresponding to the C–F stretching mode for the S–enantiomer of CHBrClF.

q	HF	B3LYP	B-LYP	LDA
−3.00	−1.4057	−0.9236	−0.5863	−0.4649
−2.50	−1.2602	−0.7835	−0.4606	−0.3314
−2.00	−1.1226	−0.6493	−0.3406	−0.2040
−1.50	−0.9935	−0.5213	−0.2263	−0.0826
−1.00	−0.8736	−0.3999	−0.1179	+0.0326
−0.50	−0.7632	−0.2856	−0.0155	+0.1413
−0.25	−0.7116	−0.2312	+0.0334	+0.1932
−0.125	−0.6868	−0.2047	+0.0573	+0.2185
+0.00	−0.6625	−0.1787	+0.0807	+0.2434
+0.125	−0.6388	−0.1531	+0.1037	+0.2678
+0.25	−0.6157	−0.1280	+0.1264	+0.2919
+0.50	−0.5714	−0.0793	+0.1704	+0.3386
+1.00	−0.4899	+0.0125	+0.2536	+0.4267
+1.50	−0.4176	+0.0964	+0.3300	+0.5074
+2.00	−0.3542	+0.1724	+0.3993	+0.5803
+2.50	−0.2995	+0.2406	+0.4613	+0.6449
+3.00	−0.2529	+0.3007	+0.5157	+0.7008

Table 1.6: Vibrational term values G_n corresponding to the one dimensional cut through the CCSD(T) parity conserving potential energy hypersurface (G_n in cm^{-1}) for the C–F stretching mode of the S–enantiomer of CHBrClF, giving $\tilde{\nu} = 1103.6\,\mathrm{cm}^{-1}$.

n	G_n
0	558.8
1	1662.4
2	2748.2
3	3816.4
4	4868.5
5	5912.1
6	6971.5
7	8086.2

Table 1.7: Vibrational expectation values $\langle n|q^k|n\rangle$ of the dimensionless reduced normal coordinates q corresponding to the one dimensional cut through the CCSD(T) parity conserving potential energy hypersurface in a given state v for the C–F stretching mode of the S–enantiomer of CHBrClF.

n	$k=0$	$k=1$	$k=2$	$k=3$	$k=4$	$k=5$
0	1	0.10096×10^0	0.51622×10^0	0.18849×10^0	0.81721×10^0	0.57233×10^0
1	1	0.30477×10^0	0.16184×10^1	0.12523×10^1	0.45968×10^1	0.57639×10^1
2	1	0.51112×10^0	0.28254×10^1	0.34731×10^1	0.13389×10^2	0.24235×10^2
3	1	0.71912×10^0	0.41379×10^1	0.69425×10^1	0.28654×10^2	0.67272×10^2
4	1	0.92082×10^0	0.55304×10^1	0.11609×10^2	0.51380×10^2	0.14568×10^3
5	1	0.10780×10^1	0.68564×10^1	0.16677×10^2	0.79283×10^2	0.25494×10^3
6	1	0.11147×10^1	0.77943×10^1	0.20041×10^2	0.10337×10^3	0.35242×10^3
7	1	0.10091×10^1	0.81859×10^1	0.20229×10^2	0.11553×10^3	0.39079×10^3

Table 1.8: Polynomial fit coefficients p_j and root mean square deviation d_{RMS} (all in $10^{-12}\mathrm{cm}^{-1}$) for the S–enantiomer of CHBrClF. The standard deviations due to the fit procedure are given in parenthesis in units of the last significant digits. For HF, the fitting instead employed q^4 versus q^3 to reduce the standard error in the coefficients.

	HF	B3LYP	B-LYP	LDA
p_0	−1.4540(1)	−0.3926(2)	+0.17719(8)	+0.5344(2)
p_1	+0.42160(5)	+0.4532(3)	+0.40826(9)	+0.4334(2)
p_2	−0.04243(9)	−0.03244(5)	−0.02826(2)	−0.03054(4)
p_3	—	−0.00060(4)	−0.00057(1)	−0.00078(3)
p_4	+0.00019(1)	—	—	—
d_{RMS}	3.2×10^{-4}	7.0×10^{-4}	2.3×10^{-4}	4.7×10^{-4}

Table 1.9: Vibrationally averaged ZORA parity violating potential $E^S_{n,\mathrm{pv}}$ for energy levels v corresponding to the one dimensional cut through the CCSD(T) parity conserving potential energy hypersurface ($E^S_{n,\mathrm{pv}}$ in $10^{-12}\mathrm{cm}^{-1}hc$) for the C–F stretching mode of the S–enantiomer of CHBrClF.

n	HF	B3LYP	B-LYP	LDA
0	−1.4332	−0.3637	0.2037	0.5623
1	−1.3933	−0.3077	0.2552	0.6161
2	−1.3558	−0.2547	0.3040	0.6669
3	−1.3208	−0.2050	0.3499	0.7143
4	−1.2904	−0.1616	0.3902	0.7555
5	−1.2750	−0.1364	0.4139	0.7792
6	−1.2946	−0.1522	0.4005	0.7638
7	−1.3534	−0.2129	0.3462	0.7059

2. CHBrClI

Table 2.1: Equilibrium geometry obtained at the CCSD(T) level for the S–enantiomer of CHBrClI. Coordinates are in ångström (Å).

Atom	x	y	z
C	+0.000000	+0.000000	+0.000000
H	+0.000000	+0.000000	+1.098200
Cl	+1.697764	+0.000000	−0.534788
Br	−0.928088	+1.660119	−0.539985
I	−1.062799	−1.803614	−0.605985

Table 2.2: Parity conserving potential energy (V_{pc} in 10^3 Hartree (E_h)) evaluated at the CCSD(T) equilibrium geometry for the S–enantiomer of CHBrClI.

V_{pc}
−0.522608168

Table 2.3: ZORA parity violating potential energies (V_{pv} in 10^{-17} Hartree (E_h)) evaluated at the CCSD(T) equilibrium geometry for the S–enantiomer of CHBrClI.

HF	B3LYP	B-LYP	LDA
−11.2626	−3.5740	+1.7914	+4.0814

3. CHBrFI

Table 3.1: Equilibrium geometry obtained at the CCSD(T) level for the S–enantiomer of CHBrFI. Coordinates are in ångström (Å).

Atom	x	y	z
C	+0.729723	+0.418636	+0.571767
H	+0.729723	+0.418636	+1.672467
F	+2.009599	+0.418636	+0.116313
Br	−0.157533	+2.083409	−0.002427
I	−0.277690	−1.401241	−0.083255

Table 3.2: Unscaled harmonic wavenumbers $\tilde{\omega}$ (in cm^{-1}) calculated at the CCSD(T) level of theory for the S–enantiomer of CHBrFI. The C–F stretch mode corresponds to mode ν_4.

Mode	$\tilde{\omega}$ (cm^{-1})
ν_1	3161.3
ν_2	1319.3
ν_3	1180.3
ν_4	1101.7
ν_5	653.7
ν_6	552.3
ν_7	326.4
ν_8	267.8
ν_9	143.4

Table 3.3: Cartesian displacements (in Å) corresponding to a unit shift along the dimensionless reduced normal coordinate q_4 for the S–enantiomer of CHBrFI.

Atom	x	y	z
C	-6.7015×10^{-1}	-1.5302×10^{-2}	$+2.7789 \times 10^{-1}$
H	-3.9417×10^{-1}	$+8.8959 \times 10^{-2}$	$+2.9062 \times 10^{-1}$
F	$+4.3849 \times 10^{-1}$	$+5.2807 \times 10^{-3}$	-1.8275×10^{-1}
Br	$+1.2460 \times 10^{-3}$	$+1.0871 \times 10^{-3}$	-7.9624×10^{-4}
I	$+8.0518 \times 10^{-5}$	-7.2608×10^{-4}	-7.3047×10^{-4}

Table 3.4: One dimensional cut through the CCSD(T) parity conserving potential energy hypersurface (V_{pc} in 10^3 Hartree (E_h)) along the dimensionless reduced normal coordinate (q_4) corresponding to the C–F stretching mode for the S–enantiomer of CHBrFI.

q	V_{pc}	q	V_{pc}
−5.00	−0.162444020	+0.05	−0.162578987
−4.50	−0.162478539	+0.10	−0.162578968
−4.00	−0.162505916	+0.15	−0.162578938
−3.50	−0.162527382	+0.20	−0.162578895
−3.00	−0.162543950	+0.25	−0.162578841
−2.80	−0.162549401	+0.30	−0.162578776
−2.60	−0.162554251	+0.35	−0.162578700
−2.40	−0.162558545	+0.40	−0.162578613
−2.20	−0.162562323	+0.45	−0.162578515
−2.00	−0.162565624	+0.50	−0.162578407
−1.80	−0.162568481	+0.55	−0.162578289
−1.60	−0.162570929	+0.60	−0.162578161
−1.50	−0.162572009	+0.65	−0.162578023
−1.40	−0.162572997	+0.70	−0.162577875
−1.30	−0.162573898	+0.75	−0.162577718
−1.20	−0.162574714	+0.80	−0.162577553
−1.10	−0.162575449	+0.85	−0.162577378
−1.00	−0.162576106	+0.90	−0.162577194
−0.95	−0.162576406	+0.95	−0.162577002
−0.90	−0.162576688	+1.00	−0.162576801
−0.85	−0.162576951	+1.10	−0.162576376
−0.80	−0.162577197	+1.20	−0.162575919
−0.75	−0.162577426	+1.30	−0.162575432
−0.70	−0.162577638	+1.40	−0.162574917
−0.65	−0.162577833	+1.50	−0.162574374
−0.60	−0.162578011	+1.60	−0.162573806
−0.55	−0.162578174	+1.80	−0.162572595
−0.50	−0.162578321	+2.00	−0.162571293
−0.45	−0.162578452	+2.20	−0.162569909
−0.40	−0.162578569	+2.40	−0.162568450
−0.35	−0.162578670	+2.60	−0.162566924
−0.30	−0.162578758	+2.80	−0.162565337
−0.25	−0.162578831	+3.00	−0.162563695
−0.20	−0.162578890	+3.50	−0.162559390
−0.15	−0.162578935	+4.00	−0.162554858
−0.10	−0.162578968	+4.50	−0.162550164
−0.05	−0.162578987	+5.00	−0.162545362
+0.00	−0.162578993		

Table 3.5: One dimensional cut through the ZORA parity violating potential energy hypersurface (V_{pv} in 10^{-16} Hartree (E_h)) along the dimensionless reduced normal coordinate (q_4) corresponding to the C–F stretching mode for the S–enantiomer of CHBrFI.

q	HF	B3LYP	B-LYP	LDA
−3.00	−2.9287	−1.5363	−0.6330	−0.3206
−2.50	−2.7037	−1.3152	−0.4239	−0.0925
−2.00	−2.4904	−1.1057	−0.2271	+0.1223
−1.50	−2.2889	−0.9066	−0.0409	+0.3257
−1.00	−2.0991	−0.7169	+0.1362	+0.5192
−0.50	−1.9209	−0.5355	+0.3055	+0.7044
−0.25	−1.8361	−0.4478	+0.3877	+0.7942
−0.125	−1.7947	−0.4046	+0.4281	+0.8384
+0.00	−1.7540	−0.3619	+0.4681	+0.8822
+0.125	−1.7140	−0.3196	+0.5078	+0.9257
+0.25	−1.6747	−0.2777	+0.5471	+0.9687
+0.50	−1.5981	−0.1952	+0.6248	+1.0537
+1.00	−1.4527	−0.0350	+0.7763	+1.2193
+1.50	−1.3177	+0.1192	+0.9229	+1.3794
+2.00	−1.1924	+0.2679	+1.0650	+1.5341
+2.50	−1.0767	+0.4112	+1.2026	+1.6834
+3.00	−0.9702	+0.5492	+1.3353	+1.8267

Table 3.6: Vibrational term values G_n corresponding to the one dimensional cut through the CCSD(T) parity conserving potential energy hypersurface (G_n in cm^{-1}) for the C–F stretching mode for the S–enantiomer of CHBrFI, giving $\tilde{\nu} = 1082.5\,\mathrm{cm}^{-1}$.

n	G_n
0	548.6
1	1631.1
2	2695.1
3	3740.9
4	4770.0
5	5791.2
6	6830.5
7	7928.2

Table 3.7: Vibrational expectation values $\langle n|q^k|n\rangle$ of the dimensionless reduced normal coordinates q corresponding to the one dimensional cut through the CCSD(T) parity conserving potential energy hypersurface in a given state n for the C–F stretching mode of the S–enantiomer of CHBrFI.

n	$k=0$	$k=1$	$k=2$	$k=3$	$k=4$	$k=5$
0	1	0.10138×10^{0}	0.51632×10^{0}	0.18944×10^{0}	0.81776×10^{0}	0.57563×10^{0}
1	1	0.30694×10^{0}	0.16198×10^{1}	0.12615×10^{1}	0.46078×10^{1}	0.58104×10^{1}
2	1	0.51503×10^{0}	0.28299×10^{1}	0.35019×10^{1}	0.13442×10^{2}	0.24464×10^{2}
3	1	0.72472×10^{0}	0.41469×10^{1}	0.70035×10^{1}	0.28803×10^{2}	0.67967×10^{2}
4	1	0.92774×10^{0}	0.55442×10^{1}	0.11710×10^{2}	0.51681×10^{2}	0.14719×10^{3}
5	1	0.10847×10^{1}	0.68704×10^{1}	0.16798×10^{2}	0.79678×10^{2}	0.25717×10^{3}
6	1	0.11192×10^{1}	0.77993×10^{1}	0.20131×10^{2}	0.10362×10^{3}	0.35428×10^{3}
7	1	0.10113×10^{1}	0.81798×10^{1}	0.20269×10^{2}	0.11551×10^{3}	0.39161×10^{3}

Table 3.8: Polynomial fit coefficients p_j and root mean square deviation d_{RMS} (all in $10^{-12}\mathrm{cm}^{-1}$) for the S–enantiomer of CHBrFI. The standard deviations due to the fit procedure are given in parenthesis in units of the last significant digits.

	HF	B3LYP	B-LYP	LDA
p_0	−38.4959(5)	−7.9426(1)	+10.2740(2)	+19.36278(5)
p_1	+7.0861(5)	+7.4637(1)	+7.0016(2)	+7.66025(5)
p_2	−0.4820(4)	−0.3064(1)	−0.2572(1)	−0.28146(4)
p_3	+0.00875(8)	+0.01829(2)	+0.02204(2)	+0.021593(7)
p_4	+0.00060(5)	−0.00162(1)	−0.00312(1)	−0.003720(4)
d_{RMS}	1.4×10^{-3}	3.4×10^{-4}	4.3×10^{-4}	1.3×10^{-4}

Table 3.9: Vibrationally averaged ZORA parity violating potential $E^S_{n,\mathrm{pv}}$ for energy levels n corresponding to the one dimensional cut through the CCSD(T) parity conserving potential energy hypersurface ($E^S_{n,\mathrm{pv}}$ in $10^{-12}\mathrm{cm}^{-1}hc$) for the C–F stretching mode of the S–enantiomer of CHBrFI.

n	HF	B3LYP	B-LYP	LDA
0	−38.007	−7.324	+10.869	+20.013
1	−37.044	−6.085	+12.064	+21.317
2	−36.102	−4.846	+13.261	+22.617
3	−35.185	−3.615	+14.448	+23.902
4	−34.345	−2.455	+15.566	+25.105
5	−33.815	−1.647	+16.343	+25.935
6	−34.016	−1.700	+16.300	+25.871
7	−34.993	−2.685	+15.368	+24.848

4. CHClFI

Table 4.1: Equilibrium geometry obtained at the CCSD(T) level for the *S*–enantiomer of CHClFI. Coordinates are in ångström (Å).

Atom	x	y	z
C	+0.675746	+0.938694	+0.559128
H	+0.675746	+0.938694	+1.658928
F	+1.955077	+0.938694	+0.104230
Cl	−0.147564	+2.413509	+0.006067
I	−0.321300	−0.901823	−0.083323

Table 4.2: Unscaled harmonic wavenumbers $\tilde{\omega}$ (in cm^{-1}) calculated at the CCSD(T) level of theory for the *S*–enantiomer of CHClFI. The C–F stretch mode corresponds to mode ν_4.

Mode	$\tilde{\omega}$ (cm^{-1})
ν_1	3162.1
ν_2	1327.8
ν_3	1210.3
ν_4	1108.2
ν_5	776.2
ν_6	576.4
ν_7	413.0
ν_8	269.5
ν_9	193.5

Table 4.3: Cartesian displacements (in Å) corresponding to a unit shift along the dimensionless reduced normal coordinate q_4 for the *S*–enantiomer of CHClFI.

Atom	x	y	z
C	-6.4891×10^{-1}	-7.7498×10^{-3}	$+2.5848 \times 10^{-1}$
H	-4.1203×10^{-1}	$+2.5406 \times 10^{-1}$	$+2.7089 \times 10^{-1}$
F	$+4.1629 \times 10^{-1}$	$+8.2713 \times 10^{-3}$	-1.7567×10^{-1}
Cl	$+8.8691 \times 10^{-3}$	-5.2195×10^{-3}	$+2.8526 \times 10^{-3}$
I	-1.3346×10^{-4}	-1.0849×10^{-3}	-1.0806×10^{-3}

Table 4.4: One dimensional cut through the CCSD(T) parity conserving potential energy hypersurface (V_{pc} in 10^3 Hartree (E_h)) along the dimensionless reduced normal coordinate (q_4) corresponding to the C–F stretching mode of the S–enantiomer of CHClFI.

q	V_{pc}	q	V_{pc}
−5.00	−0.608940357	+0.05	−0.609074330
−4.50	−0.608974488	+0.10	−0.609074312
−4.00	−0.609001603	+0.15	−0.609074281
−3.50	−0.609022899	+0.20	−0.609074238
−3.00	−0.609039366	+0.25	−0.609074184
−2.80	−0.609044790	+0.30	−0.609074118
−2.60	−0.609049620	+0.35	−0.609074041
−2.40	−0.609053899	+0.40	−0.609073953
−2.20	−0.609057667	+0.45	−0.609073854
−2.00	−0.609060961	+0.50	−0.609073745
−1.80	−0.609063815	+0.55	−0.609073626
−1.60	−0.609066261	+0.60	−0.609073497
−1.50	−0.609067341	+0.65	−0.609073357
−1.40	−0.609068330	+0.70	−0.609073209
−1.30	−0.609069231	+0.75	−0.609073050
−1.20	−0.609070048	+0.80	−0.609072883
−1.10	−0.609070784	+0.85	−0.609072706
−1.00	−0.609071442	+0.90	−0.609072521
−0.95	−0.609071743	+0.95	−0.609072327
−0.90	−0.609072025	+1.00	−0.609072124
−0.85	−0.609072289	+1.10	−0.609071694
−0.80	−0.609072536	+1.20	−0.609071232
−0.75	−0.609072765	+1.30	−0.609070740
−0.70	−0.609072977	+1.40	−0.609070219
−0.65	−0.609073173	+1.50	−0.609069670
−0.60	−0.609073352	+1.60	−0.609069094
−0.55	−0.609073515	+1.80	−0.609067867
−0.50	−0.609073662	+2.00	−0.609066547
−0.45	−0.609073794	+2.20	−0.609065143
−0.40	−0.609073911	+2.40	−0.609063662
−0.35	−0.609074013	+2.60	−0.609062112
−0.30	−0.609074101	+2.80	−0.609060498
−0.25	−0.609074174	+3.00	−0.609058828
−0.20	−0.609074233	+3.50	−0.609054441
−0.15	−0.609074279	+4.00	−0.609049813
−0.10	−0.609074311	+4.50	−0.609045009
−0.05	−0.609074330	+5.00	−0.609040084
+0.00	−0.609074337		

Table 4.5: One dimensional cut through the ZORA parity violating potential energy hypersurface (V_{pv} in 10^{-16} Hartree (E_h)) along the dimensionless reduced normal coordinate (q_4) corresponding to the C–F stretching mode for the *S*–enantiomer of CHClFI.

q	HF	B3LYP	B-LYP	LDA
−3.00	−1.3204	−0.7209	−0.3237	−0.2308
−2.50	−1.1875	−0.6144	−0.2396	−0.1408
−2.00	−1.0609	−0.5125	−0.1599	−0.0554
−1.50	−0.9412	−0.4153	−0.0842	+0.0257
−1.00	−0.8287	−0.3227	−0.0124	+0.1026
−0.50	−0.7234	−0.2350	+0.0556	+0.1754
−0.25	−0.6735	−0.1929	+0.0881	+0.2103
−0.125	−0.6492	−0.1723	+0.1041	+0.2273
+0.00	−0.6248	−0.1520	+0.1198	+0.2441
+0.125	−0.6021	−0.1321	+0.1352	+0.2607
+0.25	−0.5791	−0.1124	+0.1504	+0.2770
+0.50	−0.5346	−0.0740	+0.1802	+0.3088
+1.00	−0.4508	−0.0010	+0.2368	+0.3694
+1.50	−0.3739	+0.0672	+0.2896	+0.4258
+2.00	−0.3035	+0.1303	+0.3386	+0.4779
+2.50	−0.2395	+0.1884	+0.3834	+0.5253
+3.00	−0.1818	+0.2413	+0.4241	+0.5678

Table 4.6: Vibrational term values G_n corresponding to the one dimensional cut through the CCSD(T) parity conserving potential energy hypersurface (G_n in cm^{-1}) for the C–F stretching mode for the *S*–enantiomer of CHClFI, giving $\tilde{\nu} = 1089.9\,\mathrm{cm}^{-1}$.

n	G_n
0	552.0
1	1642.0
2	2714.0
3	3768.5
4	4807.0
5	5837.2
6	6883.8
7	7986.0

Table 4.7: Vibrational expectation values $\langle n|q^k|n\rangle$ of the dimensionless reduced normal coordinates q corresponding to the one dimensional cut through the CCSD(T) parity conserving potential energy hypersurface in a given state n for the C–F stretching mode for the S–enantiomer of CHClFI.

n	$k=0$	$k=1$	$k=2$	$k=3$	$k=4$	$k=5$
0	1	0.10138×10^{0}	0.51632×10^{0}	0.18944×10^{0}	0.81776×10^{0}	0.57563×10^{0}
1	1	0.30694×10^{0}	0.16198×10^{1}	0.12615×10^{1}	0.46078×10^{1}	0.58104×10^{1}
2	1	0.51503×10^{0}	0.28299×10^{1}	0.35019×10^{1}	0.13442×10^{2}	0.24464×10^{2}
3	1	0.72472×10^{0}	0.41469×10^{1}	0.70035×10^{1}	0.28803×10^{2}	0.67967×10^{2}
4	1	0.92774×10^{0}	0.55442×10^{1}	0.11710×10^{2}	0.51681×10^{2}	0.14719×10^{3}
5	1	0.10847×10^{1}	0.68704×10^{1}	0.16798×10^{2}	0.79678×10^{2}	0.25717×10^{3}
6	1	0.11192×10^{1}	0.77993×10^{1}	0.20131×10^{2}	0.10362×10^{3}	0.35428×10^{3}
7	1	0.10113×10^{1}	0.81798×10^{1}	0.20269×10^{2}	0.11551×10^{3}	0.39161×10^{3}

Table 4.8: Polynomial fit coefficients p_j and root mean square deviation d_{RMS} (all in $10^{-12}\mathrm{cm}^{-1}$) for the S–enantiomer of CHClFI. The standard deviations due to the fit procedure are given in parenthesis in units of the last significant digits. In B3LYP the q^4 coefficient had a large standard deviation and a fit to a third order polynomial was instead employed.

	HF	B3LYP	B-LYP	LDA
p_0	$-13.725(2)$	$-3.3376(2)$	$+2.62823(6)$	$+5.35813(5)$
p_1	$+4.146(2)$	$+3.5330(3)$	$+2.73442(6)$	$+2.92957(4)$
p_2	$-0.317(1)$	$-0.21401(5)$	$-0.16456(4)$	$-0.17746(3)$
p_3	$+0.0022(2)$	$-0.00146(4)$	$+0.000097(9)$	$-0.000912(7)$
p_4	$+0.0011(1)$	—	$-0.000562(5)$	$-0.000774(4)$
d_{RMS}	4.1×10^{-3}	7.2×10^{-4}	1.5×10^{-4}	1.3×10^{-4}

Table 4.9: Vibrationally averaged ZORA HF parity violating potential $E^S_{n,\mathrm{pv}}$ for energy levels n corresponding to the one dimensional cut through the CCSD(T) parity conserving potential energy hypersurface ($E^S_{n,\mathrm{pv}}$ in $10^{-12}\mathrm{cm}^{-1}hc$) for the C–F stretching mode for the S–enantiomer of CHClFI.

n	HF	B3LYP	B-LYP	LDA
0	-13.467	-3.090	$+2.820$	$+5.563$
1	-12.957	-2.602	$+3.199$	$+5.965$
2	-12.463	-2.129	$+3.564$	$+6.351$
3	-11.986	-1.675	$+3.912$	$+6.717$
4	-11.551	-1.264	$+4.225$	$+7.041$
5	-11.277	-1.000	$+4.421$	$+7.240$
6	-11.395	-1.082	$+4.349$	$+7.154$
7	-11.949	-1.544	$+3.985$	$+6.761$

5. CBrClFI

Table 5.1: Equilibrium geometry obtained at the CCSD(T) level for the S–enantiomer of CBrClFI. Coordinates are in ångström (Å).

Atom	x	y	z
C	+0.000000	+0.000000	+0.000000
F	+0.000000	+0.000000	+1.353900
Cl	+1.693915	+0.000000	−0.546532
Br	−0.917624	+1.656874	−0.589073
I	−1.058457	−1.805169	−0.667896

Table 5.2: Parity conserving potential energy (V_{pc} in 10^3 Hartree (E_h)) evaluated at the CCSD(T) equilibrium geometry for the S–enantiomer of CBrClFI.

V_{pc}
−0.621634778

Table 5.3: ZORA parity violating potential energies (V_{pv} in 10^{-17} Hartree (E_h)) evaluated at the CCSD(T) equilibrium geometry for the S–enantiomer of CBrClFI.

HF	B3LYP	B-LYP	LDA
+2.3337	+0.55295	−0.4055	−1.0058

6. CHAtFI

Table 6.1: Equilibrium geometry obtained at the CCSD(T) level for the S–enantiomer of CHAtFI. Coordinates are in ångström (Å).

Atom	x	y	z
C	+0.863123	+0.513755	+0.600204
H	+0.863123	+0.513755	+1.701404
F	+2.143232	+0.513755	+0.140351
I	−0.162386	+2.314885	−0.063529
At	−0.148532	−1.470244	−0.016691

Table 6.2: Unscaled harmonic wavenumbers $\tilde{\omega}$ (in cm^{-1}) calculated at the CCSD(T) level of theory for the S–enantiomer of CHAtFI. The C–F stretch mode corresponds to mode ν_4.

Mode	$\tilde{\omega}$
ν_1	3154.0
ν_2	1305.4
ν_3	1107.7
ν_4	1091.3
ν_5	635.2
ν_6	503.7
ν_7	351.8
ν_8	240.9
ν_9	164.3

Table 6.3: Cartesian displacements (in Å) corresponding to a unit shift along the dimensionless reduced normal coordinate (q_4) for the S–enantiomer of CHAtFI.

Atom	x	y	z
C	-4.7667×10^{-1}	-6.2582×10^{-2}	$+1.8077 \times 10^{-1}$
H	-1.8105×10^{-1}	$+7.4559 \times 10^{-1}$	$+1.9151 \times 10^{-1}$
F	$+3.0958 \times 10^{-1}$	$+1.0444 \times 10^{-2}$	-1.2199×10^{-1}
I	$+1.0354 \times 10^{-3}$	-2.7812×10^{-4}	$+1.6075 \times 10^{-3}$
At	-5.2322×10^{-4}	-7.7527×10^{-4}	-1.1780×10^{-3}

Table 6.4: One dimensional cut through the CCSD(T) parity conserving potential energy hypersurface (V_{pc} in 10^3 Hartree (E_h)) along the dimensionless reduced normal coordinate (q_4) corresponding to the C–F stretching mode of the S–enantiomer of CHAtFI.

q	V_{pc}	q	V_{pc}
−5.00	−0.160192900	+0.05	−0.160315815
−4.50	−0.160223585	+0.10	−0.160315797
−4.00	−0.160248179	+0.15	−0.160315767
−3.50	−0.160267664	+0.20	−0.160315725
−3.00	−0.160282862	+0.25	−0.160315671
−2.80	−0.160287899	+0.30	−0.160315606
−2.60	−0.160292400	+0.35	−0.160315530
−2.40	−0.160296402	+0.40	−0.160315442
−2.20	−0.160299938	+0.45	−0.160315344
−2.00	−0.160303041	+0.50	−0.160315236
−1.80	−0.160305739	+0.55	−0.160315117
−1.60	−0.160308061	+0.60	−0.160314988
−1.50	−0.160309088	+0.65	−0.160314848
−1.40	−0.160310031	+0.70	−0.160314699
−1.30	−0.160310892	+0.75	−0.160314540
−1.20	−0.160311675	+0.80	−0.160314372
−1.10	−0.160312381	+0.85	−0.160314194
−1.00	−0.160313014	+0.90	−0.160314007
−0.95	−0.160313303	+0.95	−0.160313812
−0.90	−0.160313575	+1.00	−0.160313607
−0.85	−0.160313831	+1.10	−0.160313171
−0.80	−0.160314069	+1.20	−0.160312701
−0.75	−0.160314291	+1.30	−0.160312199
−0.70	−0.160314496	+1.40	−0.160311666
−0.65	−0.160314686	+1.50	−0.160311102
−0.60	−0.160314860	+1.60	−0.160310508
−0.55	−0.160315018	+1.80	−0.160309237
−0.50	−0.160315162	+2.00	−0.160307859
−0.45	−0.160315290	+2.20	−0.160306382
−0.40	−0.160315404	+2.40	−0.160304811
−0.35	−0.160315504	+2.60	−0.160303152
−0.30	−0.160315590	+2.80	−0.160301411
−0.25	−0.160315661	+3.00	−0.160299593
−0.20	−0.160315720	+3.50	−0.160294735
−0.15	−0.160315765	+4.00	−0.160289479
−0.10	−0.160315796	+4.50	−0.160283872
−0.05	−0.160315815	+5.00	−0.160277952
+0.00	−0.160315822		

Table 6.5: One dimensional cut through the ZORA parity violating potential energy hypersurface (V_{pv} in 10^{-14} Hartree (E_h)) along the dimensionless reduced normal coordinate (q_4) corresponding to the C–F stretching mode for the S–enantiomer of CHAtFI.

q	HF	B3LYP	B-LYP	LDA
−3.00	−1.5323	−0.4835	−0.0071	+0.1472
−2.50	−1.3835	−0.3623	+0.1035	+0.2576
−2.00	−1.2674	−0.2714	+0.1857	+0.3381
−1.50	−1.1799	−0.2068	+0.2431	+0.3928
−1.00	−1.1175	−0.1650	+0.2796	+0.4256
−0.50	−1.0767	−0.1426	+0.2986	+0.4402
−0.25	−1.0635	−0.1375	+0.3025	+0.4417
−0.125	−1.0586	−0.1364	+0.3033	+0.4412
+0.00	−1.0546	−0.1361	+0.3033	+0.4400
+0.125	−1.0517	−0.1367	+0.3026	+0.4381
+0.25	−1.0497	−0.1380	+0.3013	+0.4355
+0.50	−1.0484	−0.1427	+0.2970	+0.4285
+1.00	−1.0555	−0.1593	+0.2826	+0.4087
+1.50	−1.0735	−0.1833	+0.2627	+0.3834
+2.00	−1.1003	−0.2123	+0.2400	+0.3553
+2.50	−1.1340	−0.2441	+0.2164	+0.3266
+3.00	−1.1728	−0.2766	+0.1940	+0.2992

Table 6.6: Vibrational term values G_n corresponding to the one dimensional cut through the CCSD(T) parity conserving potential energy hypersurface (G_n in cm^{-1}) for the C–F stretching mode of the S–enantiomer of CHAtFI, giving $\tilde{\nu} = 1080.1\,\mathrm{cm}^{-1}$.

n	G_n
0	544.6
1	1624.7
2	2694.6
3	3755.0
4	4806.7
5	5853.0
6	6905.7
7	7991.0

Table 6.7: Vibrational expectation values $\langle n|q^k|n\rangle$ of the dimensionless reduced normal coordinates q corresponding to the one dimensional cut through the CCSD(T) parity conserving potential energy hypersurface in a given state n for the C–F stretching mode of the S–enantiomer of CHAtFI.

n	$k=0$	$k=1$	$k=2$	$k=3$	$k=4$	$k=5$
0	1	0.08870×10^0	0.51126×10^0	0.16423×10^0	0.79697×10^0	0.49309×10^0
1	1	0.26515×10^0	0.15832×10^1	0.10743×10^1	0.43481×10^1	0.48442×10^1
2	1	0.44015×10^0	0.27248×10^1	0.29264×10^1	0.12274×10^2	0.19813×10^2
3	1	0.61326×10^0	0.39326×10^1	0.57460×10^1	0.25473×10^2	0.53507×10^2
4	1	0.78155×10^0	0.51946×10^1	0.95039×10^1	0.44634×10^2	0.11389×10^3
5	1	0.92887×10^0	0.64494×10^1	0.13864×10^2	0.69115×10^2	0.20280×10^3
6	1	0.10084×10^1	0.75154×10^1	0.17641×10^2	0.94328×10^2	0.30016×10^3
7	1	0.97058×10^0	0.81669×10^1	0.19157×10^2	0.11234×10^3	0.36331×10^3

Table 6.8: Polynomial fit coefficients p_j and root mean square deviation d_{RMS} (all in $10^{-12}\mathrm{cm}^{-1}$) for the S–enantiomer of CHAtFI. The standard deviations due to the fit procedure are given in parenthesis in units of the last significant digits.

	HF	B3LYP	B-LYP	LDA
p_0	−2314.67(4)	−298.79(2)	+665.64(6)	+965.70(7)
p_1	+59.91(5)	−2.32(2)	−5.37(6)	−27.67(7)
p_2	−69.50(4)	−56.81(1)	−48.41(5)	−49.86(5)
p_3	+7.948(7)	+8.671(2)	+8.776(9)	+9.26(1)
p_4	−0.351(4)	−0.296(2)	−0.307(5)	−0.335(5)
d_{RMS}	0.13	0.050	0.17	0.18

Table 6.9: Vibrationally averaged ZORA HF parity violating potential $E^S_{n,\mathrm{pv}}$ for energy levels n corresponding to the one dimensional cut through the CCSD(T) parity conserving potential energy hypersurface ($E^S_{n,\mathrm{pv}}$ in $10^{-12}\mathrm{cm}^{-1}hc$) for the C–F stretching mode for the S–enantiomer of CHAtFI.

n	HF	B3LYP	B-LYP	LDA
0	−2343.9	−326.85	+641.61	+939.00
1	−2401.8	−381.33	+595.66	+887.91
2	−2458.7	−432.88	+553.28	+840.65
3	−2514.5	−481.36	+514.57	+797.33
4	−2569.0	−526.53	+479.68	+758.13
5	−2621.3	−567.61	+448.89	+723.67
6	−2669.4	−603.07	+422.27	+694.85
7	−2711.2	−632.19	+398.71	+671.42

7. Model Potentials

Table 7.1: Parameters of the model density for astatine used to construct the model potential in the two-component ZORA approach.

$\alpha_i^{\mathrm{mod}}/a_0^2$	c_i^{mod}
29968676.500049	0.0000778287
4311900.2819510	0.0005823416
1214858.2856859	0.0021067949
558686.50529816	0.0035165722
297718.55598697	0.0094669338
155931.55320815	0.0205646473
81515.549139827	0.0572097377
39150.803113776	0.1575355595
18802.535457056	0.3569037238
9334.053606972	0.5987004049
4814.262338303	0.5604367846
2559.012619449	−0.0503679582
1537.861561664	−0.2271830064
766.169712805	2.4872237662
461.459864496	5.5464650397
170.314774442	−16.8325640377
151.834815072	11.4545547106
78.400805776	26.3859138914
30.530952320	−50.6054634838
27.384994087	33.3690438735
14.809282479	30.9370731952
10.813458191	10.2553337949
6.075990122	−7.2669467856
3.276209638	12.7282123469
1.852975598	15.6977711054
1.438553495	−6.6951627503
1.017400759	6.8993039262
0.626094344	−3.4204465609
0.494683120	7.6489216867
0.247136186	3.1832028555
0.178754611	1.2802720250
0.101615125	0.4577410369